

Kinetic Study on Reduction of FeO in a Molten HIsarna Slag by Various Solid Carbon Sources



THEINT THEINT HTET, ZHIMING YAN, DARBAZ KHASRAW, JOHANNES HAGE, KOEN MEIJER, and ZUSHU LI

To investigate the reduction behaviour of different reductants such as charcoal (CC), thermal coal (TC), and carbon black (CB) with HIsarna slag, a series of isothermal reduction experiments were performed in a vertical tube resistance furnace (VTF), coupled with a Quadrupole mass spectrometer (QMS) at 1450 °C, 1475 °C and 1500 °C. The results confirm that the highest overall reduction rate was achieved by CC, followed by TC and CB. The reduction mechanism between FeO containing molten slag and the selected carbonaceous materials is determined by studying the morphology of the water quenched samples at the intervals of 1.5, 3 and 5 minutes, using optical and scanning electron microscopes. The results reveal that the overall reaction is controlled by two main mechanisms: (1) nucleation and growth of CO bubbles, proceeded by the gaseous intermediates CO and CO₂; and (2) diffusion of FeO in the molten slag. The initial reduction period in which chemical reaction control is dominant, can be described by the Avrami–Erofeev model, whereas the final period is described by the three-dimensional diffusion model.

<https://doi.org/10.1007/s11663-022-02677-1>
© The Author(s) 2022

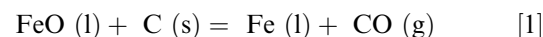
1. INTRODUCTION

HISARNA TECHNOLOGY is an alternative to blast furnace ironmaking, developed by Tata Steel IJmuiden, aiming to reduce CO₂ emissions up to 80 pct by 2050 in conjunction with carbon capture and storage (CCS) method.^[1] It involves a smelting reduction process integrated with cyclone technology, operating as a single smelting furnace.^[1,2] Melting the raw materials such as iron ore, fluxes, and pre-reduction of the ore occurs in the Cyclone Converter Furnace (CCF), located above the Smelting Reduction Vessel (SRV), where the final reduction of iron oxides takes place.^[1,2] One of the great advantages that HIsarna offers is direct use of various alternative reductants to the standard metallurgical coal in the SRV.^[2] 6 wt pct of FeO in slag is maintained in the SRV, resulting in 90 wt pct of phosphorous being partitioned into molten slag phase.^[1–4] Up to date, the process has successfully

demonstrated the capability of significantly reducing the carbon footprints using thermal coal (TC), and charcoal (CC) in a pilot plant at a capacity of 60,000 t/a.^[1–4] These previous successful campaigns open an opportunity in research to study the reduction behaviours of various carbon in molten HIsarna slag.

The fundamentals of the reaction mechanism between molten slag and solid carbon have been well established by numerous researchers,^[5–13] and the detailed mechanism is explained as follows;

- (1) Once the reaction is initiated, a gas film containing CO between the molten slag and the solid carbon emerges, resulting from the direct reduction reaction, Eq. [1].
- (2) The product CO subsequently reacts with FeO from the molten slag at the slag/gas interface, causing indirect reduction reaction, Eq. [2]. As a result, CO₂ is generated.
- (3) The generated CO₂ travels to the solid carbon surface, producing more CO for further reduction via gasification reaction, Eq. [3]. This intermediate step is also known as the boudouard reaction.^[6,8]



THEINT THEINT HTET, ZHIMING YAN, DARBAZ KHASRAW, and ZUSHU LI are with the WMG, University of Warwick, Coventry, CV4 7AL, UK. Contact e-mails: Zhiming.Yan@warwick.ac.uk, z.li.19@warwick.ac.uk JOHANNES HAGE and KOEN MEIJER are with the IJmuiden Technology Centre, PO Box 10000, 1970 CA IJmuiden, The Netherlands.

Manuscript submitted April 19, 2022; accepted October 21, 2022.



Many researchers studied^[11–17] the reduction of iron oxides in solid or molten slag by different types of carbon, and some of the studies are summarised in Table I. Most authors agree that the mass transfer of FeO in the liquid phase is the rate limiting step during slag and solid carbon reaction. Furthermore, it is reported that the gasification reaction might play a significant role during the reduction, as the reaction rate is dependent on the type of carbon in some cases.^[11,13] Hence, our initial research^[18] focused on the gasification reactivity of the alternative reductants such as thermal coal (TC) and charcoal (CC) (both of which are already used in HIsarna's trial campaigns), in comparison to carbon black (CB) which is produced through an alternative route, to explore the effect of their physical-chemical properties on the reactivity at different temperatures. It has been established that the reactivity of CC is the highest, followed by TC and CB.^[18]

The current research focuses on an in-depth study of the reduction behaviours of those carbonaceous materials in the HIsarna slag at the temperature range of 1450 °C to 1500 °C. The experiments were conducted in a vertical tube resistance furnace (VTF) to investigate the influence of temperature and reductants on the molten HIsarna slag-carbon reaction kinetic. The reaction mechanism was studied by the kinetic curve obtained from the online off-gas data, optical micrographs, and SEM/EDS images of the quenched samples. Finally, reaction control mechanisms are explained by two models: (1) Random nucleation and growth (Avrami–Erofeev); and (2) Three-dimensional diffusion model.

II. EXPERIMENTAL

A. Materials Preparation

The synthetic HIsarna slag was made from high purity powders of CaO, MgO, SiO₂, and Al₂O₃ (Sigma-Aldrich, 99.99 pct) and FeO (Sigma-Aldrich, 99.995 pct). Its composition is presented in Table II, which is similar to the composition of HIsarna slag provided by Tata Steel Europe after excluding minor components. First, the oxide mixture of CaO, MgO, SiO₂, and Al₂O₃ was heated to 1500 °C in a muffle furnace and kept to homogenise for one hour. Then, the molten slag was quenched with water. The quenched slag was dried and crushed into powder using a TEMA disc mill with stainless steel mill plates. Finally, 6 wt pct FeO (Sigma-Aldrich) was added to the pre-melted oxide mixture at the room temperature to ensure that the FeO is not oxidised.

The crushed particles (69–90 µm) of carbonaceous materials were studied in current work, since crushed particles are injected using a carrier gas in the HIsarna process. The physical-chemical characteristic of the selected carbonaceous materials (CC, TC and CB) were thoroughly studied in our previous work^[14] and their

compositions are presented in Table III. The crushed particles of TC and CC were heated in a horizontal tube furnace to 1300 °C under an argon atmosphere at the heating rate of 10°C/min and held for 3 h to fully remove the volatiles, hence the effect of volatiles on the reduction kinetic is neglected. The volatile components of CB are negligible, since it is produced at 1450 °C.

B. Apparatus

All reduction experiments were carried out isothermally in a SiC resistance vertical tube furnace (VTF), shown schematically in Figure 1. The top and bottom ends of the tube were fitted with water-cooled flanges to protect the O-rings of both ends. A B-type thermocouple was inserted from the bottom of the furnace and sat underneath the sample holder. Tapered alumina crucible (31φ × 25 φ × 45 mm) containing slag and carbon powder mixture was held by molybdenum wire inside the alumina tube (inner diameter 88 φ × 1060 mm).

The off-gas evolving from the reaction is analysed continuously from the top of the furnace by using an online Quadrupole Mass Spectrometer (HPR20, HIDEN Analytical). A non-return valve is fitted to the top exhaust of the furnace to maintain an inert atmosphere in the furnace.

C. Experimental Procedure

Three grams of sample, consisting of slag and carbon at the 1:1 molar ratio of FeO and Carbon, were thoroughly mixed and placed in an alumina crucible. The crucible with the experimental sample was hanged initially at the top of the reaction tube (quench zone) using molybdenum wire as shown in Figure 1. Argon (N5, 99.999 pct) at the flow rate of 1L/min was then introduced to the VTF through the bottom lance to achieve the inert atmosphere inside the furnace for the reduction experiments. Meanwhile, the VTF was heated to the selected temperatures of 1450 °C, 1475 °C and 1500 °C at 12 °C/min. The off-gas of the VTF was monitored from the top of the reaction tube, using a Quadrupole Mass Spectrometer. The inert atmosphere inside the tube was achieved within 10 minutes of introducing the argon gas. Once the hot zone, in which the temperature was controlled within ± 5 °C had reached and held for 10 minutes at the selected temperature, the sample was lowered to the hot zone via the wire. The evolved gases from the reaction were recorded by QMS at every 15 seconds. The sample was kept in the hot zone isothermally until the reaction ended to study the reduction kinetics of slag with various carbon sources. In another set of experiment, the samples were quenched under argon at the intervals of 1.5, 3 and 5 minutes by rapidly removing the sample from the hot zone to the top quench zone as shown in Figure 1. The morphologies of the quenched samples were observed using an optical microscope (VHX-S750E, Keyence) and SEM/EDS (ZEISS-Sigma) to investigate the reaction mechanism of the slag-carbon reactions. The experimental method used in this study is different from HIsarna's operation, where solid carbon is injected into

Table I. Summary of the Reduction of Iron Oxides in Molten Slag by Different Types of Carbon

Sources	Method	Type of Reductants	Slag System	T (°C)	E (kJ/mol)	Findings
Bafghi <i>et al.</i> ^[5]	ethylenediaminetetraacetic acid titration (EDTA)	graphite crucible	SiO ₂ -CaO-Li ₂ O-Al ₂ O ₃ -FeO FeO: 10 wt pct basicity: 1-2	1300	—	the reduction rate is significantly influenced by the slag basicity. The reaction is controlled by mass transfer in the slag phase, when the basicity is 2, whereas the chemical reaction resistance is dominant at lower basicity
Sarma <i>et al.</i> ^[6]	sensitive pressure transducer of CO evolution	graphite coke coal char	CaO-SiO ₂ -Al ₂ O ₃ -FeO FeO: < 10 wt pct	1400 to 1450	—	the study claims that the reaction rate is non-linearly dependent on the FeO contents in slag. The reduction rate could be improved by additional factors such as external stirring of the carbon rod, encouraging faster diffusion of FeO in slag
Min <i>et al.</i> ^[7]	mass spectrometer technique	graphite rod	CaO-SiO ₂ -Al ₂ O ₃ -FeO FeO: 1 to 70 wt pct	1450	251	the rate limiting step is dependent on the FeO content in slag. It is claimed that the gasification reaction could be the limiting step when the activity of FeO is higher than 0.5, whereas a mixed step of gasification reaction with mass transfer of FeO in liquid phase could be considered as the rate-determining step of the reaction at activity of FeO lower than 0.5
Soe and Fruehan ^[8]	constant volume pressure increase (CVPI)	coal chars	CaO-SiO ₂ -FeO-Al ₂ O ₃ FeO: 1&3 wt pct basicity: 1.2	1450	—	the reduction of FeO is independent of the type of coal used regardless of the components i.e., volatile matter and ash. The overall reduction rate is controlled by a series of processes such as liquid phase mass transfer of FeO in slag and gas phase mass transfer, gasification reaction, direct and indirect reaction between FeO, C, and CO

Table I. continued

Sources	Method	Type of Reductants	Slag System	T (°C)	E (kJ/mol)	Findings
Siddiqi <i>et al.</i> ^[9]	sessile drop technique IR CO-CO ₂ analyser	graphite substrate	SiO ₂ -CaO-Al ₂ O ₃ -MgO-FeO FeO: 0.22 to 9.26 wt pct	1500 to 1600	112.18	the reduction rate is directly depending on the FeO wt pct in the molten slag and temperature
Jouhari <i>et al.</i> ^[10]	slag chemical analysis	graphite crucible	CaO-MgO-SiO ₂ -Al ₂ O ₃ -FeO FeO: 25 to 50 wt pct	1550 ± 25	153	the reduction reaction follows 1st order reaction. The reaction rate is directly proportional to FeO concentration, temperature, and reaction surface area
Teasdale and Hayes ^[11]	sessile drop technique	graphite coke bituminous coal anthracitic chars	FeO-CaO-Al ₂ O ₃ -SiO ₂ FeO: 10.5 wt pct	1400 to 1600	—	it is claimed that the reduction rate is influenced by the carbon type; faster reaction rate is achieved by graphite and coke than coal chars. The rate of reduction is controlled by mass transfer in the slag phase
Bhoi <i>et al.</i> ^[12]	slag chemical analysis	graphite crucible	SiO ₂ -CaO-Al ₂ O ₃ -MgO-Fe ₂ O ₃ Fe ₂ O ₃ : 20 to 40 wt pct basicity: 1 to 1.8	1400 to 1600	118	the reaction follows first order reaction, and the rate is increased with increasing FeO content in the slag, and temperature. Hence, the overall reduction is mainly controlled by liquid phase mass transfer of FeO
Maroufi <i>et al.</i> ^[13]	IR gas analyser SEM-EDS	coke rubber-derived carbon (RDC) coke-RDC blend pig iron (liquid)	Fe ₂ O ₃ -SiO ₂ -Al ₂ O ₃ - CaO-MgO-MnO Fe ₂ O ₃ : 36.2 wt pct	1550		overall reduction rate is influenced by the gasification of carbonaceous material
Leuchtenmueller <i>et al.</i> ^[14]	XRF SEM/EDX ICP-OES spark spectrometer (SPECTROMAXX)		MgO-Al ₂ O ₃ -SiO ₂ -CaO- FeO-ZnO	1320 to 1475	216 (ZnO) 191 (FeO)	reduction kinetics model is developed for the carbothermic reaction rate of FeO and ZnO in liquid slag; assuming that the reaction mainly takes place within the metal-slag boundary. It is found that higher reduction rate of ZnO is achieved compared to FeO
Khasraw <i>et al.</i> ^[15]	drop tube furnace coupled with a quadrupole mass spectrometer (DTF-QMS) X-ray Fluorescence (WDXRF)	thermal coal (TC) Charcoal (CC) Bana grass Char (BGC)	CaO-SiO ₂ -Al ₂ O ₃ - MgO-FeO FeO: 6 wt pct	1450 to 1525	first stage: 290 (TC), 229 (CC), 267 (BGC) Second stage: 265 (TC), 369 (CC), 282 (BGC)	the overall reduction involves two stages: Chemical reaction at solid/gas interface is dominant during the first stage, whereas mixed control i.e., gas diffusion, liquid phase mass transfer, chemical reaction, and carbon diffusion

Table I. continued

Sources	Method	Type of Reductants	Slag System	T (°C)	E (kJ/mol)	Findings
Yu <i>et al.</i> ^[16]	XRD SEM/EDS	graphite powder	CaO-SiO ₂ -FeO-P ₂ O ₅ FeO: 20, 33 wt pct P ₂ O ₅ : 5, 17 wt pct	1300		FeO reduction stopped within 1 h of reaction due to FeO existing in the C ₂ S-C ₃ P solid solution. In contrary, P ₂ O ₅ is continuously reduced even after 7 h

Table II. Composition of Synthetic HIsarna Slag (Wt Pct)

CaO	SiO ₂	Al ₂ O ₃	MgO	FeO
41.66	33.33	13.00	6.00	6.00

the molten slag using a carrier gas. Injecting CB nano-particles into the molten slag is not an option due to a blockage in the injection lance from preliminary experiments. Hence, a premixed sample of slag and carbon is used to compare the reaction behaviour of different carbon sources in the present research.

III. RESULTS AND DISCUSSION

A. Off-Gas Analysis

Smelting reduction of FeO in molten slag by different carbon is studied by analysing the off-gas composition (mainly CO and CO₂) during the reaction, and the results from QMS are presented in Figures 2(a) through (i). In general, both CO and CO₂ (vol pct) generated from the reaction of molten slag with all the selected reductants increase with increasing reaction temperature according to Figures 2(a) through (i). Reactions between slag and CC gives the highest CO and CO₂ volumes followed by TC and CB, at a similar time under all selected reaction temperatures, indicating that the highest FeO reduction rate is achieved with CC, whereas the lowest with CB. The peak of CO (vol pct) evolved is found to be significantly higher than CO₂ in the cases of CC and TC, Figures 2(a) through (f). However, a similar height of CO and CO₂ (vol pct) is generated during the reduction with CB, Figures 2(g) through (i).

Once the sample reaches the hot zone, the reaction is initiated through the direct reduction (Eq. [1]), leading to the formation of CO bubbles between solid carbon and slag.^[8–10] The generated CO could rapidly be used up through the indirect reaction (Eq. [2]), producing CO₂. Hence, mainly CO₂ is detected during the initial 100 seconds of the reduction. The carbon gasification reaction becomes dominant after 100 seconds, resulting in a decrease in CO₂ vol pct and an increase in CO vol/pct. Additionally, the gasification reaction is highly influenced by the temperature, and the type of the carbon.^[18,19] According to the previous work,^[18] the gasification rate of CC at the HIsarna's operating temperature is the highest followed by TC and CB. Therefore, the vol pct of CO generated during the reaction with CC is significantly higher than CO₂ compared to TC and CB. Moreover, it is apparent that there are sudden spikes occurred in CO curves of CC in Figure 2(b) and CB in Figures 2(h) and (i). This could be due to the CO bubbles rupturing during the reaction.

To investigate the reaction mechanism of the smelting reduction with the various types of carbon, the reduction degree (α), Eq. [4] is determined. Since the reduction occurs in the inert gas atmosphere, the total mole of oxygen in the off-gases (CO, CO₂) at the time t is

Table III. Proximate and Ultimate Analyses (Dry Basis) of Charcoal and Thermal Coal Provided by Tata Steel Europe, IJmuiden and the Composition of Carbon Back (Reprinted from Ref. [18], Under the Terms of the Creative Commons CC BY License)

Sample	Proximate Analysis (Wt Pct)			Ultimate Analysis (Wt Pct)				
	Volatile	Fixed Carbon	Ash	H	O	N	S	C
CC	12.1	81.5	1.8	3.1	6.9	0.57	0.1	89.4
TC	22.2	60.1	8.8	4.3	11.4	2.2	0.2	81.9

CB	Elemental Carbon	Ash Content	Organic
	> 97 pct	< 1 pct	< 1 pct

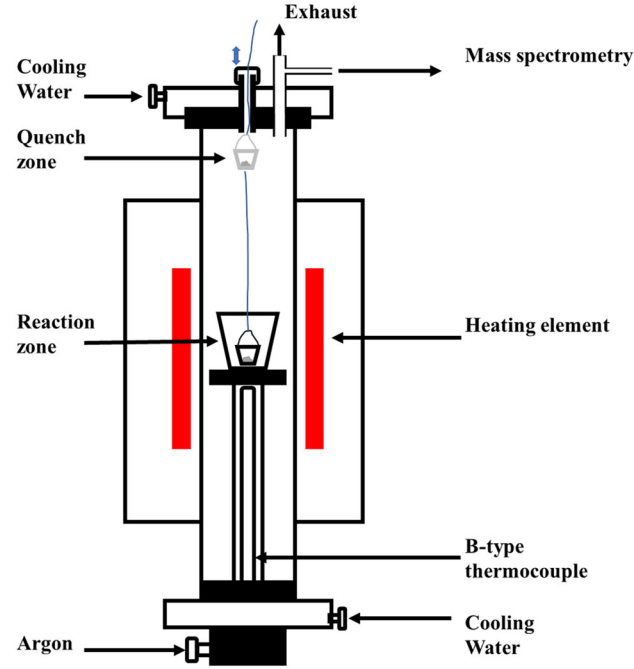


Fig. 1—Schematic diagram of the experimental set up for FeO reduction in molten slag.

considered to be from FeO. Hence, the mole of FeO in the slag at the time t can be calculated from the total mole of oxygen detected in the off-gas during the time t . The reduction degrees, resulting from reacting with CC, TC, and CB at different temperatures are presented in Figures 3(a) through (c).

$$\alpha = \frac{\text{FeO}_i - \text{FeO}_t}{\text{FeO}_i} \quad [4]$$

where α represents reduction degree; FeO_i and FeO_t are the amount of FeO in mole at the initial point and at the time t , respectively.

The reduction fraction evidently increases with raising reaction temperature for all the carbon types, as shown in Figures 3(a) through (c). Overall, the highest reduction degree is achieved by CC compared to TC and CB. The final reduction degrees with CC at three temperatures, Figure 3(a) are not significantly different while an apparent increase in the reduction degree is achieved

with the increased temperature for TC (Figure 3(b)), and CB (Figure 3(c)). The reduction degree with CB seems to be slowly increasing till 600 seconds, Figure 3(c), implying that the off-gases continuously evolved from the sample zone at a slow rate. The reason could be due to the nanoparticle, CB increases the slag viscosity, which in turn increases the bubble stability.^[20,21] This could lead to slower rupturing of the bubbles during the reaction compared to CC and TC. Consequently, the reduction degree of CB continuously increased even at 600 seconds. Furthermore, Figures 3(a) through (c) reveal that the reaction mechanism involves more than one stage as inflection points are observed on the reduction degree curve. The stages of the reaction and the reaction mechanism are determined by fitting the reduction curves with kinetic models. The detailed consideration of kinetic models is explained in Section III-B.

B. Kinetic Study

1. Kinetic models

Reaction kinetic is generally controlled by the reactant concentrations, temperature, pressure and the reactive surface area of the solid.^[22] The current study is conducted under atmospheric pressure, hence the effect of pressure on the kinetic is neglected. As the reaction occurs between the evolved gases and the solid carbon particles, the reactive surface area could not be defined, resulting in difficulty to study the reaction kinetics via the rate equations. In the case where the reaction area is uncertain, the correlation between the change in surface area of reductant and the reduction degree (α) or reactant conversion, obtained from Eq. [4] is applied.^[22] Therefore, the reduction degree curves (Figures 3(a) through (c)) present the overall reduction profile, also known as kinetic curves.

The thermal reduction rate is considered as a function of two variables, temperature T and reduction degree α .^[23]

$$\frac{d\alpha}{dt} = k(T)f(\alpha) \quad [5]$$

where k is the temperature-dependent rate constant.

The temperature reduction rate constant is determined by the Arrhenius equation.^[23]

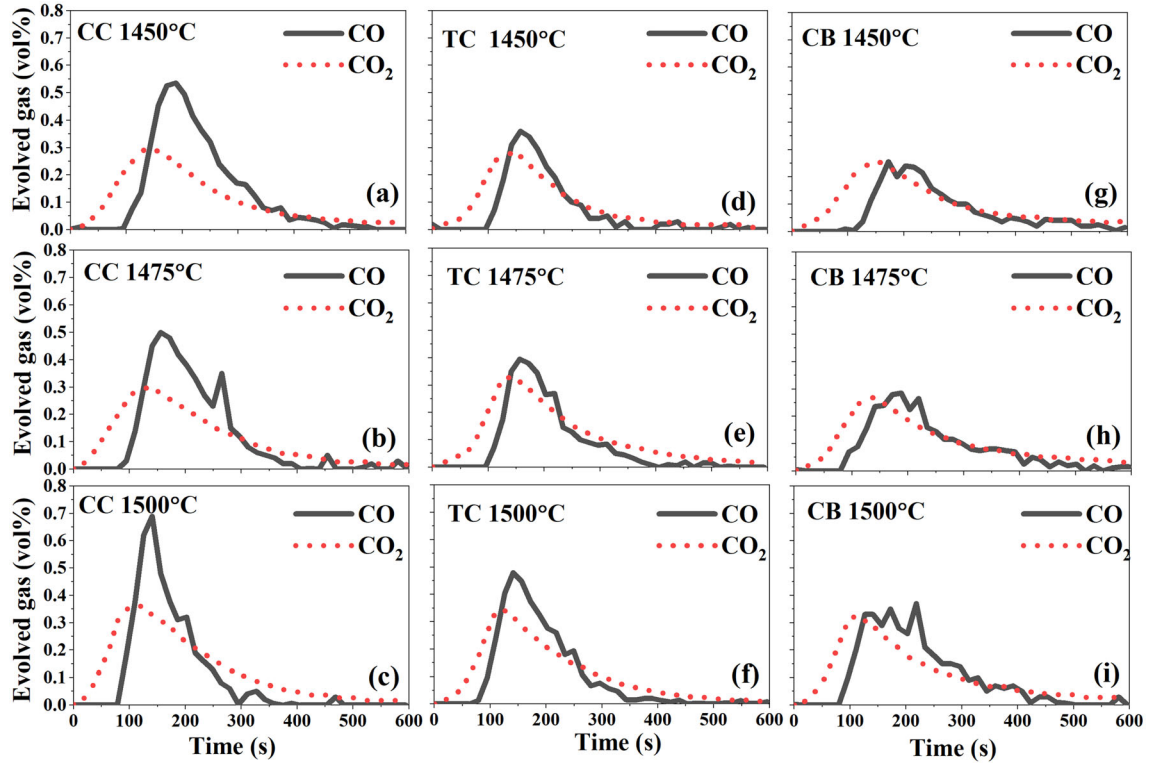


Fig. 2—The evolved gases of CO and CO₂ in vol pct during the reduction of FeO with CC (a), (b), (c); TC (d), (e), (f); CB (g), (h), (i) at 1450 °C, 1475 °C and 1500 °C respectively.

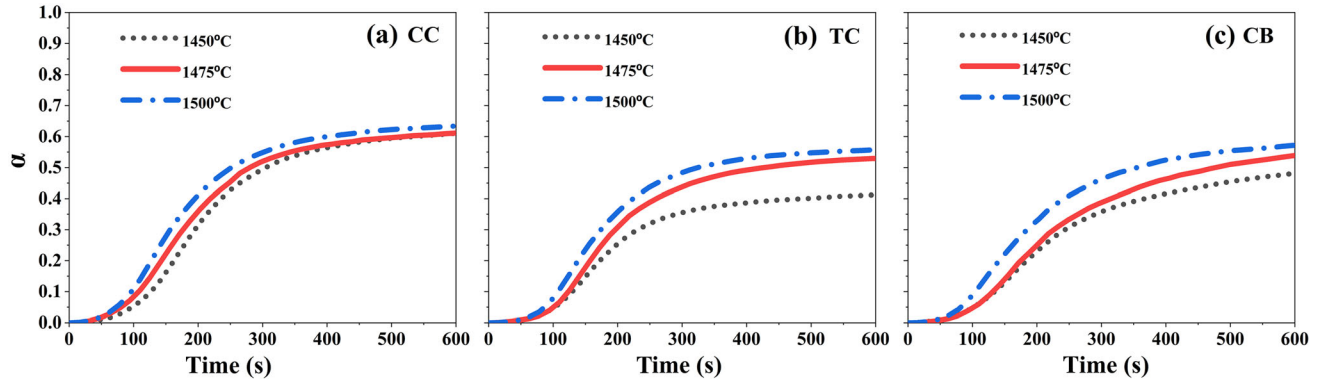


Fig. 3—Reduction degree achieved at various temperatures from the slag reacting with (a) CC, (b) TC, and (c) CB.

$$k(T) = A \exp\left(\frac{-E}{RT}\right) \quad [6]$$

where A and E are the pre-exponential factor and activation energy, respectively, and R is universal gas constant.

Under the isothermal conditions, $k(T)$ in Eq. [5] becomes constant. Hence, the rate can be described by the kinetic model, $f(\alpha)$ derived from the correlation of the surface area to the reduction degree according to Eq. [7].

$$\frac{d\alpha}{dt} \propto f(\alpha) \quad [7]$$

The reaction profiles of the current study can be classified into three distinct stages such as; Stage-1: Incubation period, Stage-2: Accelerating period, Stage-3: Decelerating period, as shown in Figure 4. The detailed mechanism occurring during the stages is discovered by the morphological study of the quenched samples at different time intervals and explained in Section III-C. The combination of stage-1 and 2 results in sigmoidal shape curve and defined as Region I.

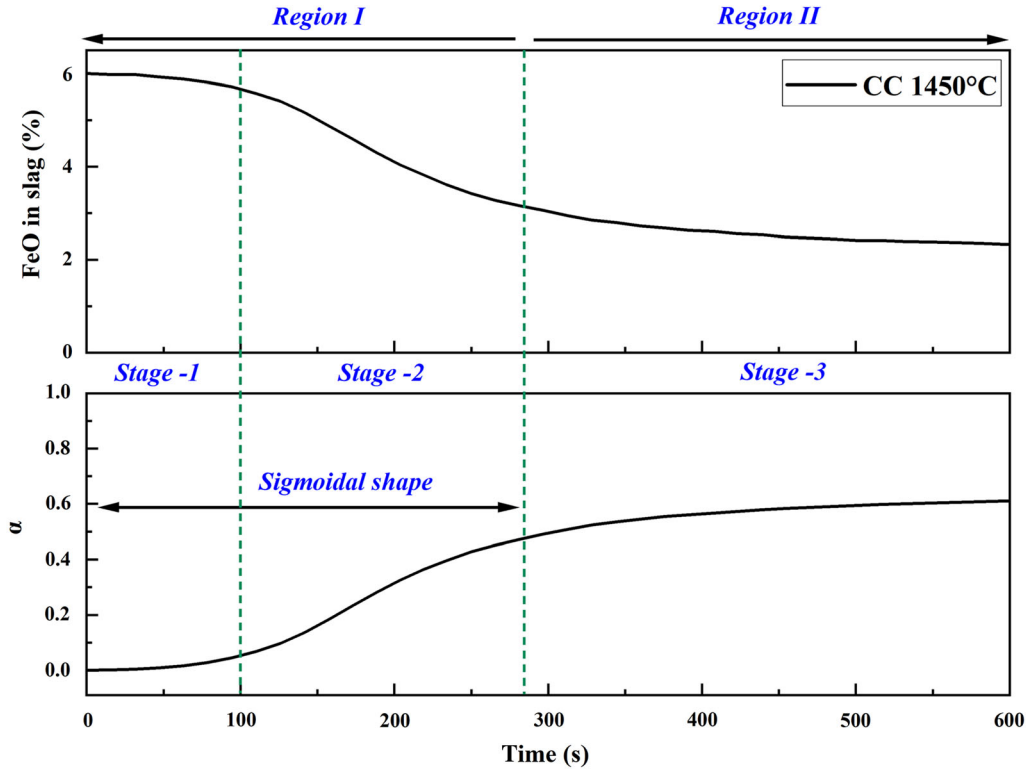


Fig. 4—Stages involved in the smelting reduction reaction, CC 1450 °C: comparison of FeO concentration (pct) in molten slag and reduction degree (α) of FeO as a function of reaction time.

Sigmoidal shape is commonly described by Avrami–Erofeev model (Random nucleation and growth), Eq. [8] in thermal reduction reactions.^[23–25]

Moreover, Basu and Ray^[25] applied Avrami–Erofeev model to study the smelting reduction of iron oxide rich slags under various conditions such as temperature, basicity. Paramguru *et al.*^[26] also claims that the reduction of FeO in CaO–SiO₂–FeO slag by solid carbon could be described by Avrami–Erofeev model with an n value of greater than 1. Hence, Avrami–Erofeev model is selected to study the Region I of the current study. The differential form of the model is presented in Eq. [8].

$$f(\alpha) = n(1 - \alpha)[- \ln(1 - \alpha)]^{(n-1)/n} \quad [8]$$

$g(\alpha)$ represents the integral form of the kinetic model.

$$g(\alpha) = \int_0^{\alpha} \frac{d\alpha}{f(\alpha)} = k(T) \int_0^t dt \quad [9]$$

$$g(\alpha) = [- \ln(1 - \alpha)]^{1/n} = kt \quad [10]$$

where n is an Avrami exponent.

Region II in Figure 4 shows a decelerating profile as the increment of the reduction degree (α) is not significant compared to Region I. Diffusion models are known to describe the decelerating behaviour.^[19,20] Three-dimensional diffusion model known as Jander

equation, Eq. [11], is considered for Region II, since it has been applied for the diffusion controlled reduction in the past study.^[23,27]

$$g(\alpha) = [1 - (1 - \alpha)^{1/3}]^2 = kt \quad [11]$$

2. Model fitting

Avrami exponent, n , could be obtained by taking the logarithm on both sides of Eq. [10].^[28]

$$\ln[- \ln(1 - \alpha)] = n \ln t + n \ln k \quad [12]$$

According to Eq. [12], the slope of the ln–ln graph gives the value of the Avrami exponent. Hence, ln–ln plots of experimental data are determined and presented in Figures 5(a) through (i). It is apparent that the reaction involves two main mechanisms, as the whole process is fitted with two significant linear fittings, as shown in Figures 5(a) through (i). The n values obtained from the linear fittings of the first mechanism lie between 2 and 3, which are used for solving the Avrami–Erofeev model, Eq. [10].

Furthermore, to ascertain the rate constant of each region, Avrami–Erofeev and Diffusion models are plotted for Region I and II based on the experimental data. It is found that there is a good linear relationship in the plots for Region I, as shown in Figures 6(a) through (i) with the coefficient determination (R^2) value of above 0.97. This confirms that Region I is governed by nucleation and growth model (Avrami–Erofeev). On the other hand, the fitting results for TC, Figures 7(a)

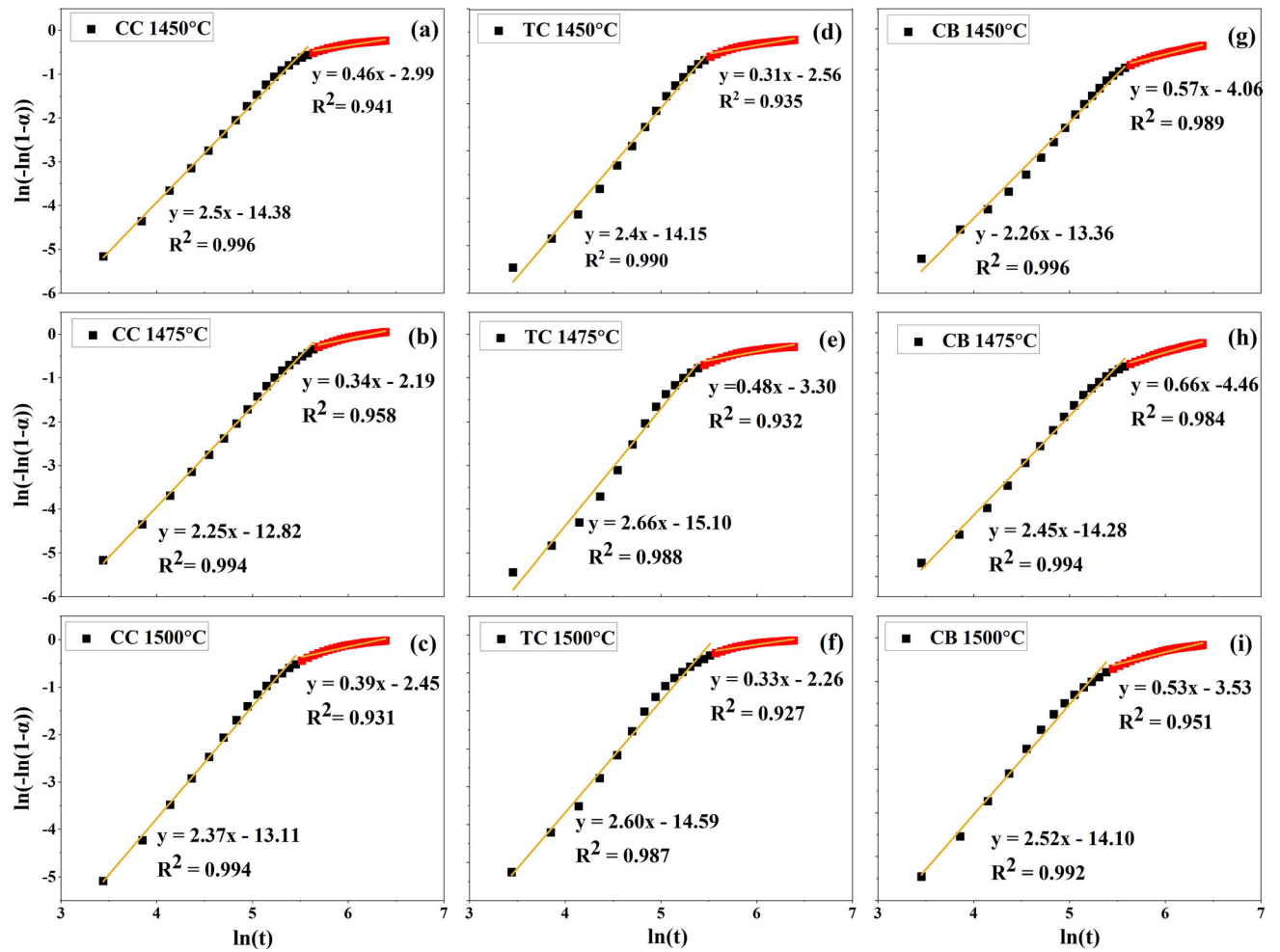


Fig. 5—ln-ln plots of experimental data (a) CC 1450 °C, (b) CC 1475 °C, (c) CC 1500 °C, (d) TC 1450 °C, (e) TC 1475 °C, (f) TC 1500 °C, (g) CB 1450 °C, (h) CB 1475 °C, and (i) CB 1500 °C.

through (c) and CC, Figures 7(d) through (f) in Region II do not have as good linear relationship as CB, Figures 7(g) through (i), as R^2 values are between 0.90 and 0.94. The regions are divided by choosing the mid-point of the transition period. Hence, this could be due to the slower transition period for TC and CC compared to CB. Being nano-particles, CB particles could be carried by the gas bubbles faster compared to the other two types of carbon, reaching to diffusion stage quicker. The kinetic parameters obtained from both models are displayed in Table IV, and the values increase with increasing temperature due to achieving faster reaction rate at higher temperature.

Activation energy values of Region-I and Region-II could be obtained from plotting the natural logarithm of the calculated rate constants against inverse temperature. The calculated values of activation energy for Region-I and Region-II are displayed in Figures 8(a) and (b), respectively. It is commonly known that the higher the activation energy, the slower the reaction rate is achieved. According to Figure 8(a), CC gives the highest reduction rate with the lowest activation energy of 47 kJ/mol, followed by TC with 76 kJ/mol and CB with 89 kJ/mol in Region-I. This result agrees well with

the gasification reactivity series of the same reductants, which are thoroughly studied in our previous work.^[18] Therefore, gasification reaction plays a vital role in Region-I. On the other hand, the activation energy values of Region-II do not follow the reactivity of the reductants, since the reaction could be dominated by mass transfer of FeO from molten slag to the gas/liquid interface. The activation energy of reduction with CB is the lowest in Region-II, 123 kJ/mol, as shown in Figure 8(b). It could be due to higher FeO concentration in the molten slag during the Region-II period, resulting in a faster mass transfer rate compared to the other two reductants. However, reaction with TC in Region-II gives the highest activation energy, 431 kJ/mol, even though the concentration of FeO in the slag is higher than the reaction with CC. This could be due to the ash content of TC, 8.8 wt pct, which is much higher than CC's ash content, 1.8 wt pct.^[18] Once the slag melts, the ash containing high acidic oxides (alumina and silica) in the reductants could dissolve in the slag, resulting in viscous slag,^[29,30] which could potentially affect the mass transfer of FeO. Therefore, the diffusion rate of FeO in the slag is the slowest with TC, followed by CC and CB, respectively.

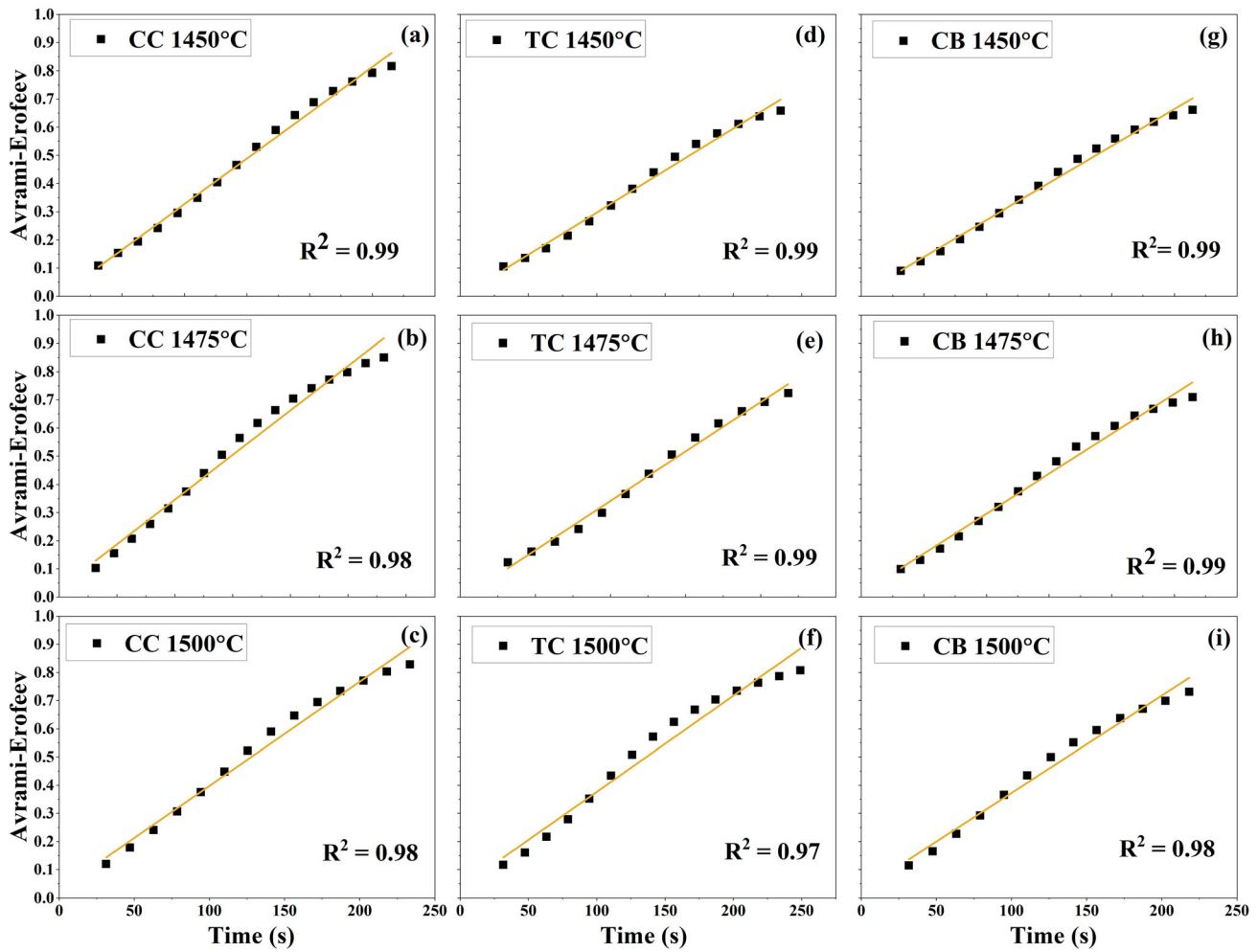


Fig. 6—Avrami-Erofeev model plots with linear fitting (a) CC 1450 °C, (b) CC 1475 °C, (c) CC 1500 °C, (d) TC 1450 °C, (e) TC 1475 °C, (f) TC 1500 °C, (g) CB 1450 °C, (h) CB 1475 °C, and (i) CB 1500 °C.

C. Morphological Study

The reaction mechanism is further assisted by studying the morphology of the quenched samples, using an optical microscope and SEM/EDS methods. During the initial 100 seconds of the reaction, the slag mixture is expected to be in a semi-molten state, generating CO_2 only and the volume of CO_2 is at maximum according to Figures 2(a) through (i). After 100 seconds, the reaction accelerates in a steady state as CO evolves and reaches to the peak approximately at 200 seconds. Then, the reaction decelerates as implied by the decreasing volume of CO and CO_2 as shown in Figures 2(a) through (i). Hence, the quenched samples are obtained at the intervals of 1.5, 3, and 5 minutes to examine the mechanisms that occurred during the three stages.

The reaction mechanism is explained with the illustrated diagrams as well as the example optical micrographs of the quenched samples (slag-TC) in Figures 9(a) through (c). Furthermore, the distribution of the carbon particles and the molten iron droplets within the molten slag at the intervals of 1.5 minutes,

3 m ins and 5 minutes were confirmed by SEM/EDS and the results are displayed in Figures 10(a) through (c).

According to the optical micrographs and SEM/EDS images of the samples, the reaction process for the slag-carbon mixture is described in the following steps:

- (1) Stage 1: The mixture is rapidly heated and reaching to the reaction temperature once it reaches the hot zone. However, the sample is still in a solid/semi-molten state in this stage. Once the reaction is initiated, CO bubble evolves at each nucleation site (*i.e.* contact area between carbon and slag), resulting from direct reduction, leading to nucleation and growth of the bubbles. Those bubbles rapidly reacts with FeO in slag, producing CO_2 gas. Hence, a lot of tiny gas bubbles are spreading throughout the slag and carbon mixture as Figure 9(a). The carbon particle lying on the gas bubbles are further confirmed by the SEM/EDS image, Figure 10(a).
- (2) Stage 2: The sample becomes fully molten in this stage, and the nucleation and growth of the bubble continues, while the reduction reaction proceeds via the gaseous intermediates, CO- CO_2 . As the reduc-

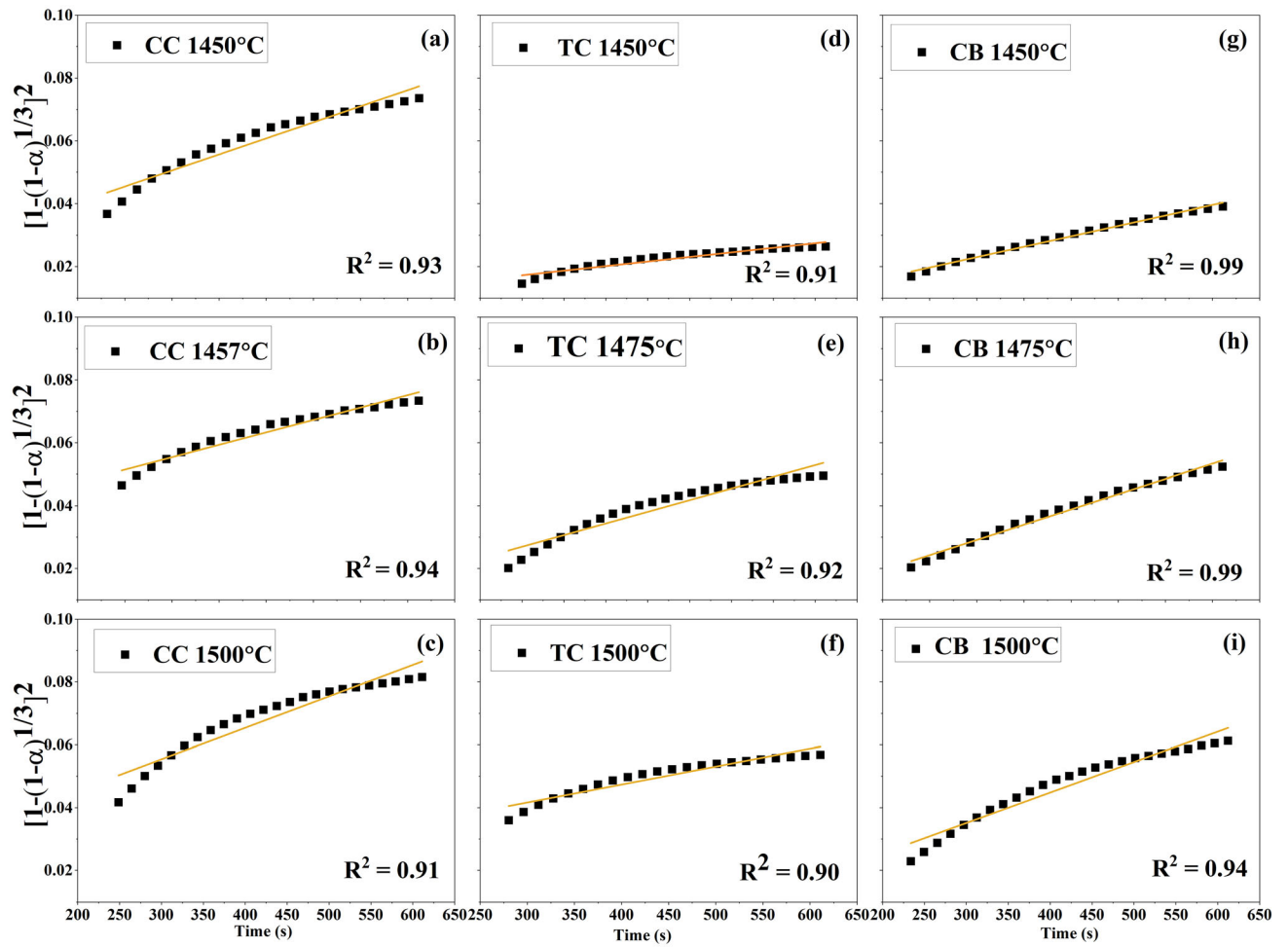


Fig. 7—Three-dimensional diffusion model plots with linear fitting (a) CC 1450 °C, (b) CC 1475 °C, (c) CC 1500 °C, (d) TC 1450 °C, (e) TC 1475 °C, (f) TC 1500 °C, (g) CB 1450 °C, (h) CB 1475 °C, (i) CB 1500 °C.

tion progresses, the bubble generation becomes significant, resulting in bubble clusters and slag foaming. The bubbles carrying carbon particles and iron droplets float to the top of the slag surface. Hence, carbon particles as well as the iron droplets (shiny particles) are found on the wall of the bubbles Figures 9(b) and 10(b).

- (3) Stage 3: The bubbles developed in stage 2 ultimately ruptured, and consequently carbon and iron droplets are deposited on the top surface of the molten slag, as observed in Figure 9(c), and the top view of

Figure 10(c). According to the vertical cross-sectional image of the sample shown in Figure 10(C), there is a negligible amount of carbon within the slag compared to the top surface. As a result, the reaction could only be proceeded via FeO diffusion in the liquid slag to the surface of the slag where most of the carbon particles are. This mechanism is further proved by determining the FeO concentration, using EDS analysis at two different locations of the cross-sectioned sample; locations are marked in Figure 10(c). According to EDS results, FeO con-

Table IV. Kinetic Parameters Obtained from Avrami–Erofeev and Three-Dimensional Diffusion Models

Reductants	Temperature (°C)	Avrami_Erofeev Model (Region I)	Three-Dimensional Diffusion Model (Region II)
		k ($s^{-1} \times 10^{-3}$)	k ($s^{-1} \times 10^{-5}$)
CC	1450	3.1	7.5
	1475	3.3	9.0
	1500	3.4	10.0
TC	1450	2.8	3.0
	1475	3.2	5.0
	1500	3.3	7.0
CB	1450	2.6	5.5
	1475	2.8	6.5
	1500	3.1	7.0

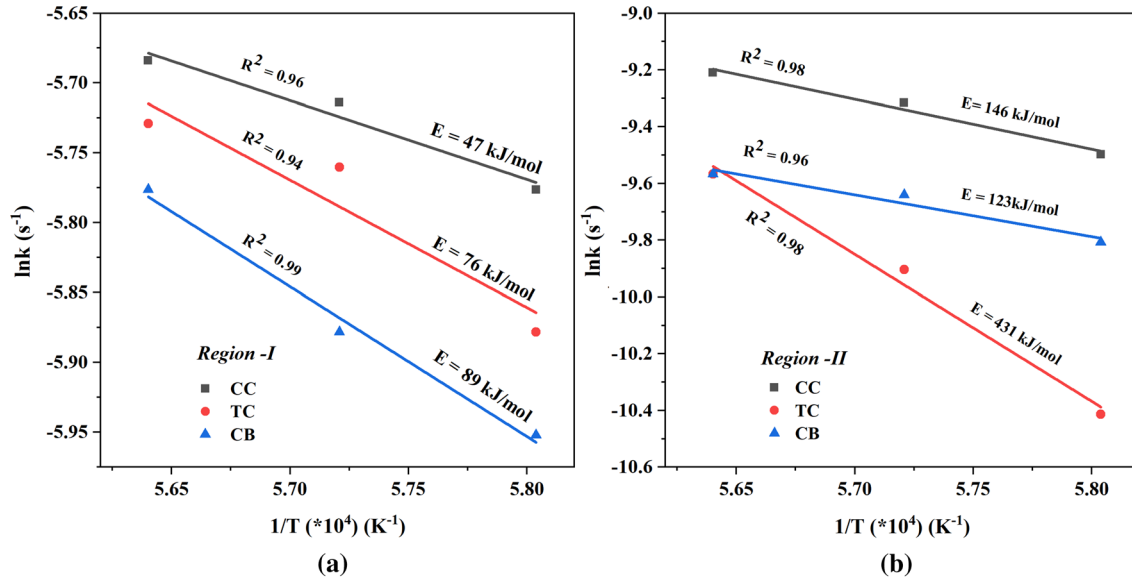


Fig. 8—Determination of activation energy from Arrhenius plots of (a) Region I (b) Region II.

centration near the surface of the liquid slag, Location-1 is 1.2 wt pct and the bottom of the crucible, Location-2 is 2.1 wt pct, proving that there is a concentration driving force for FeO diffusion in the liquid phase to occur.

The reaction mechanism in this study differs from the previous studies,^[5,9,12] which claim that the mass transfer of FeO in the slag is the main rate control step. In the current research, powder form of reductants is used and distributed in the slag mixture initially, providing an

immediate contact between FeO and the reductants. Hence, the nucleation and growth of bubbles, resulted from the gasification reaction could be dominating the reaction initially. Once carbon particles and metal droplets are floated to the top of the molten slag due to the bubbles, the reaction is influenced by the diffusion of FeO from the molten slag to the surface of the molten slag. Therefore, it could be concluded that the overall reaction is governed by two main mechanisms. The decelerating stage (*i.e.* three-dimensional diffusion

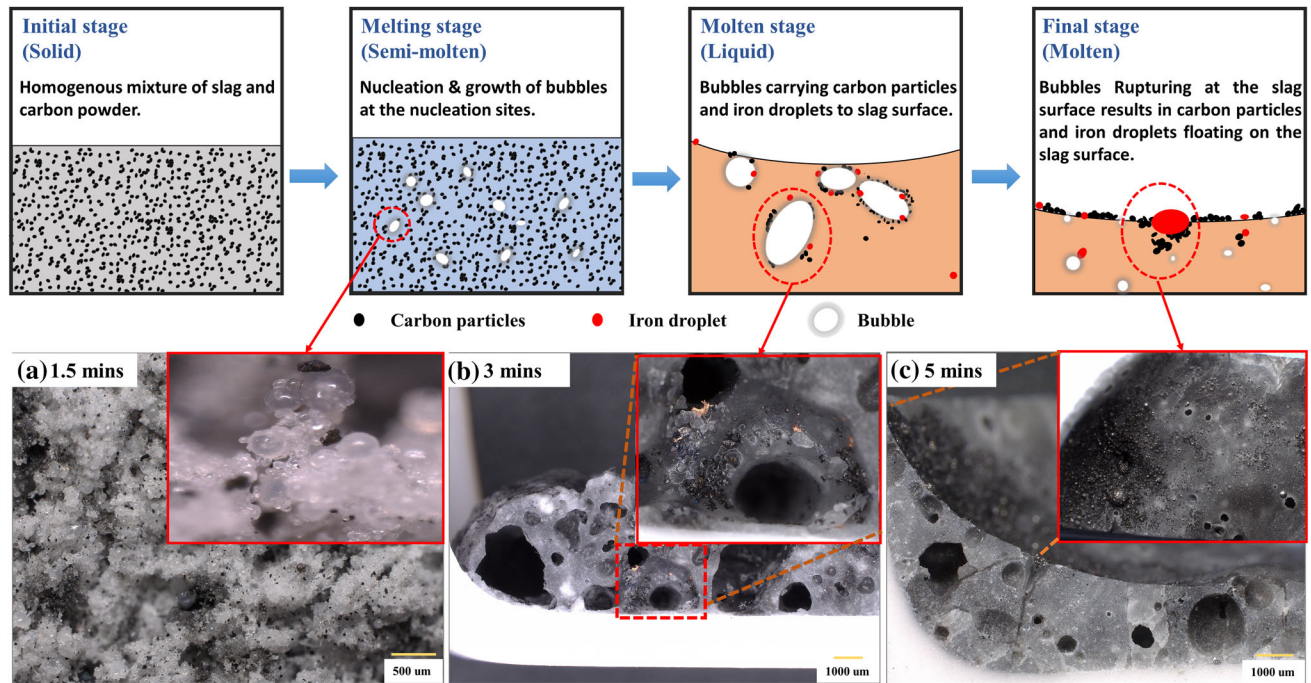


Fig. 9—Illustration of the reaction mechanism between molten slag and carbon with the micrographs of exemplary quenched samples (slag-TC system) at the intervals of (a) 1.5 min, (b) 3 min and (c) 5 min.

mechanism) found in the present research may not occur in HIsarna process because slag FeO content in HIsarna process has been constantly maintained to a higher level (approx. 6 pct) in which FeO diffusion process may not be a limiting step. This also could be due to a good distribution of solid carbon (nucleation sites) in the molten slag throughout the process resulting from a continuous stirring of molten slag and iron by the carrier gas and evolved gases. Random nucleation and growth of product gas bubbles which in turn effects the gasification and reduction reaction rate could be the main reaction mechanism between solid and molten slag in the HIsarna process. Despite the current experimental method is not identical to the HIsarna process, it reveals the reduction ability of the various carbonaceous materials.

IV. CONCLUSION

The reduction behaviours of three different reductants, CC, TC, and CB with synthetic HIsarna slag are studied in isothermal kinetic analysis, and the following conclusions could be drawn:

- (1) Under the experimental conditions, the smelting reduction rate of FeO in a molten synthetic HIsarna slag is dependent on the type of carbon and temperature. The obtained reduction rate is in the descending order of $CC > TC > CB$. Moreover, increased reduction rate and reduction degree are achieved with the increasing reaction temperature for all the selected reductants.
- (2) The overall reduction kinetic could be governed by two main steps. Initially, it is controlled by random nucleation and growth of product gas (CO , CO_2) bubbles (Region-I), followed by the diffusion of FeO from bulk molten slag to the gas/slag interface (Region II).
- (3) The reaction mechanism is further confirmed by morphological observation of exemplary quenched samples at the intervals of 1.5, 3 and 5 minutes. The slag is in semi-molten state during the first 1.5 minutes, and tiny gas bubbles growing from each nucleating sites (contact area between carbon and slag) could be seen throughout the slag. These bubbles continuously grow, carrying carbon particles and iron droplets, while the reaction progresses. Hence large bubbles, in which carbon particles and iron droplets are found in the quenched samples taken at 3 minutes. Most of the carbon particles and

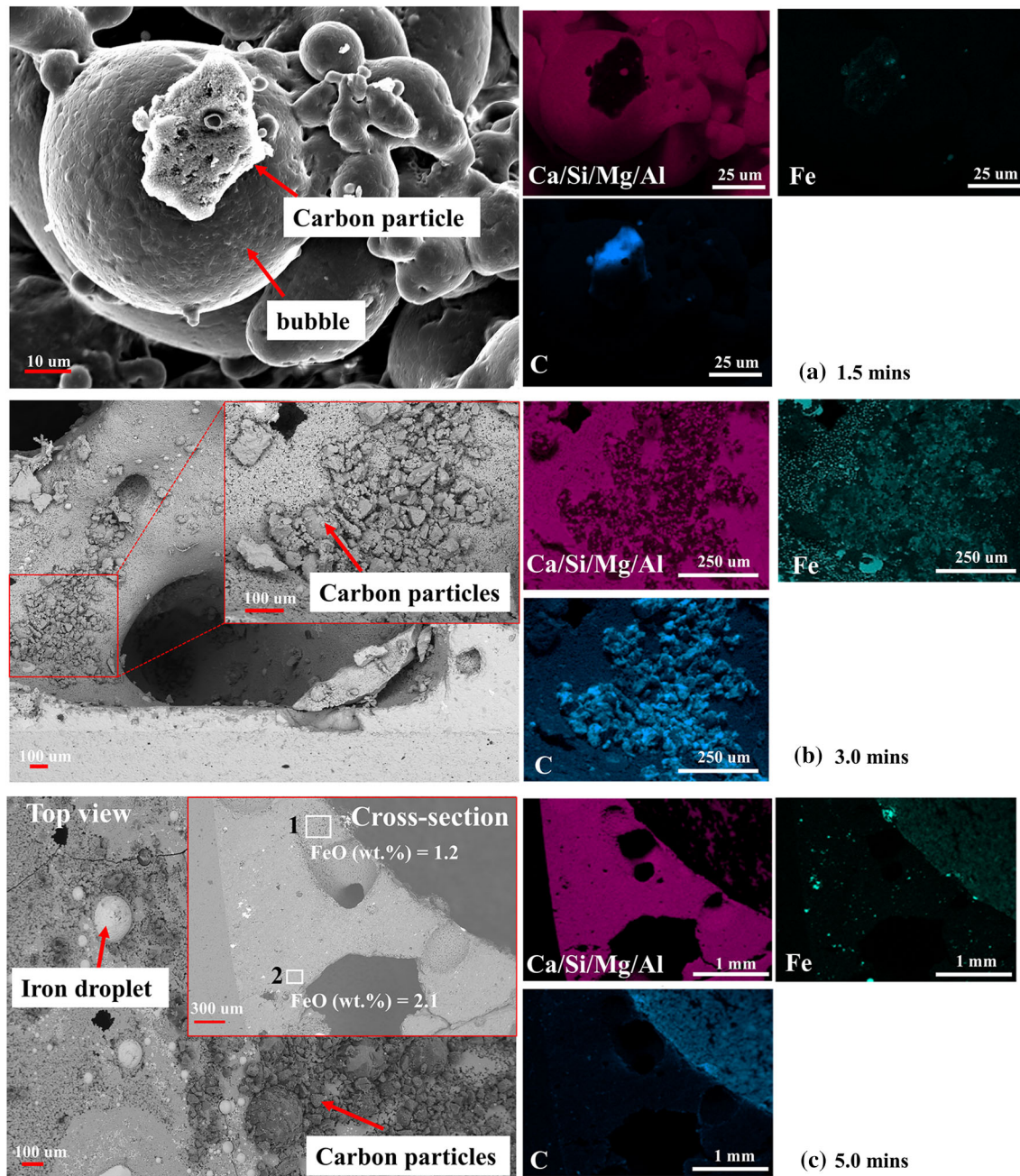


Fig. 10—SEM images and EDS maps of element distribution of the quenched samples (Slag-TC) at the intervals of (a) 1.5 min, (b) 3 min and (c) 5 min.

iron droplets are seen at the top of the slag in the 5 minutes quenched sample. This would encourage the reaction mechanism to shift from the nucleation and growth model to the diffusion model.

ACKNOWLEDGMENTS

Theint-Theint Htet highly appreciates Tata Steel Europe in IJmuiden for the full PhD studentship. Zushu Li would like to acknowledge the financial support from EPSRC under the grant number EP/N011368/1 (EPSRC Fellowship).

CONFLICT OF INTEREST

On behalf of all authors, the corresponding author states that there is no conflict of interest.

OPEN ACCESS

This article is licensed under a Creative Commons Attribution 4.0 International License, which permits use, sharing, adaptation, distribution and reproduction in any medium or format, as long as you give appropriate credit to the original author(s) and the source, provide a link to the Creative Commons licence, and indicate if changes were made. The images or other third party material in this article are included in the article's Creative Commons licence, unless indicated otherwise in a credit line to the material. If material is not included in the article's Creative Commons licence and your intended use is not permitted by statutory regulation or exceeds the permitted use, you will need to obtain permission directly from the copyright holder. To view a copy of this licence, visit <http://creativecommons.org/licenses/by/4.0/>.

REFERENCES

1. K. Meijer, C. Guenther, and R. Dry, Hisarna Pilot Plant Project. TATA steel, Netherlands, Hismelt Corp, Kwinana, Australia, pp.1–5, <https://docplayer.net/34533120-Hisarna-pilot-plant-project.html>. Accessed 22 Feb 2019.
2. J. van der Stel, K. Meijer, S. Santos, T. Peeters, and P. Broersen, in *Proceedings of the EMECR 2017 1st International Conference on Energy and Material Efficiency and CO₂ Reduction in the Steel Industry*, Kobe, Japan, 11–13 Oct 2017.
3. J. van der Stel, K. Meijer, C. Terrhuis, C. Zaijstra, G. Keilman, and M. Ouwehand, IEAGHG/IETS Iron and steel Industry CCUS and Process Integration Workshop Tokyo, Japan 4–7 Nov 2013.
4. J. van der Stel, K. Meijer, S. Santos, T. Peeters, and P. Broersen, Cato Meets Projects, December 4, 2018.
5. M. Bafghi, Y. Ito, S. Yamada, and M. Sano: *ISIJ Int.*, 1992, 32, vol. 12, pp. 1280–86.
6. B. Sarma, A. Cramb, and R. Fruehan: *Metall Mater Trans. B*, 1996, 27, vol. 5B, pp. 717–30.
7. D. Min, J. Han, and W. Chung: *Metall Mater Trans. B*, 1999, 30, vol. 2B, pp. 215–21.
8. K. Seo and R. Fruehan: *ISIJ Int.*, 2000, 40, vol. 1, pp. 7–15.
9. N. Siddiqi, B. Bhoi, R. Paramguru, V. Sahajwalla, and O. Ostrovski: *Ironmak. Steelmak.*, 2000, 27, vol. 6, pp. 437–41.
10. A. Jouhari, R. Galgali, P. Chattopadhyay, R. Gupta, and H. Ray: *Scand. J. Metall.*, 2001, 30, vol. 1, pp. 14–20.
11. S. Teasdale, and P. Hayes: *ISIJ Int.*, 2005, 45, vol. 5, pp. 642–50.
12. B. Bhoi, A.K. Jouhari, H.S. Ray, and V.N. Misra: *Ironmak. Steelmak.*, 2006, 33, vol. 3, pp. 245–52.
13. S. Maroufi, M. Mayyas, I. Mansuri, P. O’Kane, C. Skidmore, Z. Jin, A. Fontana, and V. Sahajwalla: *Metall Mater Trans. B*, 2017, 48, vol. 5, pp. 2316–23.
14. M. Leuchtenmueller, W. Schatzmann, and S. Steinlechner: *Journal of Environmental Chemical Engineering*, 2020, 4, vol. 8, pp. 103976–81.
15. D. Khasraw, Z. Yan, J.L.T. Hage, K. Meijer, and Z. Li: *Metall Mater Trans. B*, 2022, 53, vol. 5B, pp. 3246–61.
16. H. Yu, T. Miki, Y. Sasaki, and T. Nagasaka: *Metall Mater Trans. B*, 2022, vol. 53B, pp. 1806–15.
17. J. Yang, F. Firsch, and I. Sohn: *Resources Conserv. Recycl.*, 2022, vol. 178, pp. 106021–39.
18. T. Htet, Z. Yan, S. Spooner, V. Degirmenci, K. Meijer, and Z. Li: *Fuel*, 2021, vol. 289, pp. 119890–99.
19. N. Sadhwani, S. Adhikari, and M. Eden: *Ind. Eng. Chem. Res.*, 2016, 55, vol. 10, pp. 2883–91.
20. A. Lahiri, R. Yogambha, P. Dayal, and S. Seetharaman: *High Temp. Mater. Processes*, 2003, vol. 22(5–6), pp. 345–52.
21. R. Almeida, D. Vieira, W. Bielefeldt, and A. Vilela: *Mater. Res.*, 2017, 20, vol. 2, pp. 474–80.
22. H. Grénman, T. Salmi, and D. Murzin: *Rev. Chem. Eng.*, 2011, 27, vol. 1–2, pp. 53–77.
23. S. Vyazovkin, A. Burnham, J. Criado, L. Pérez-Maqueda, C. Popescu, and N. Sbirrazzuoli: *Thermochim. Acta*, 2011, 520, vol. 1–2, pp. 1–19.
24. C. Bamford and C. Tipper: *Compr. Chem. Kinet.*, 1980, vol. 22, pp. 74–84.
25. P. Basu, and H. Ray: *J. Therm. Anal*, 1995, 45, vol. 6, pp. 1533–40.
26. R. Paramguru, H. Ray, and A. Jouhari: *Ironmak. Steelmak.*, 1996, 23, vol. 5, pp. 411–15.
27. W. Lv, S. Zhao, R. Elliott, X. Lv, and M. Barati: *JOM*, 2020, 72, vol. 10, pp. 3393–3400.
28. W. Lv, X. Lv, Y. Zhang, S. Li, K. Tang, and B. Song: *Powder Technol.*, 2017, vol. 320, pp. 239–48.
29. Z. Yan, X. Lv, Z. Pang, W. He, D. Liang, C. Bai: *Metall Mater Trans. B*, 2017., 48, vol. 2B, pp. 1092–99.
30. K.C. Mills, and S. Sridhar: *Ironmak. Steelmak.*, 1999, 26, vol. 4, pp. 262–68.

Publisher’s Note Springer Nature remains neutral with regard to jurisdictional claims in published maps and institutional affiliations.